Atmospheric clearing of solid particle debris using femtosecond filaments

Kyle S. Latty* and Kyle C. Hartig
Nuclear Engineering Program, Department of Materials Science and Engineering, University of Florida, Gainesville, FL 32611, USA
(Dated: July 16, 2024)

Through nonlinear self-focusing, femtosecond pulses can propagate several kilometers beyond diffraction limits, forming an ionization channel in air known as a laser filaments. It has been demonstrated that in the wake of the filament, aerosols can be effectively cleared to improve the transmission of subsequent laser pulses or secondary light sources, pertinent to applications in atmospheric sensing. However, the current understanding of aerosol clearing is founded on interactions with droplets to simulate fogs and clouds, and thus do not extend to solid particles or atmospheric debris. Using optical trapping, we isolate both graphite and silica microparticles and directly measure the subsequent displacement caused by the filament using time-resolved shadowgraphy. The shockwave from the filament is demonstrated to propel particles away from the filament, directly contributing to atmospheric debris clearing. Particles exposed to the laser light in either the intense filament core or the surrounding energy reservoir are axially displaced along the beam path. It is found that the optomechanical properties of the particle largely influences the axial displacement induced by laser exposure through mechanisms such as radiation pressure, mass ejection from ablation or optical damage, and particle de-agglomeration.

I. INTRODUCTION

Femtosecond lasers show promise as a means of achieving standoff atmospheric sensing through the formation of laser filaments. Filamentation typically occurs through the propagation of high-power ultrashort pulses in a transparent media to achieve nonlinear self-focusing [1]. For air propagation, self-focusing causes the pulse intensity to gradually increase, eventually resulting in the ionization of air species to form a weak plasma that begins to de-focus the pulse. The dynamic balance between nonlinear self-focusing and plasma de-focusing creates a weakly ionized plasma channel in air known as a laser filament, consisting of two distinct regions: (1) the high-intensity filament core approximately 80-100 µm in diameter, capable of causing photoionization of air species to induce plasma formation [2, 3], and (2) the low-intensity energy reservoir surrounding the filament core that retains most of the pulse energy and actively restores the energy lost in the filament core [4, 5]. The intensity of the filament core is clamped given the sustained balance between self-focusing and plasma de-focusing and is sufficiently intense to excite aerosols to facilitate emission spectroscopy techniques [6–9]. Along with filament-induced particle emissions, the self-transforming white-light generated through self-phase modulation is well-suited for light detection and ranging (LIDAR) to measure absorption and scattering from air species for the purpose of atmospheric monitoring[10–13].

An underlying challenge of atmospheric monitoring using filaments or other laser-based techniques are the energy losses that accrue through scattering and absorption with atmospheric particles, attenuating light delivery and light collection at longer distances. Clouds and fogs consisting of micrometer-sized droplets are a common scattering medium in the atmosphere, inspiring several investigations dedicated to understanding the dynamics of filamentation in aerosolized environments. Filaments have been shown to survive interactions with large droplets that occlude the majority of the filament core, indicating laser filaments can persist through atmospheric attenuation as long as sufficient power resides in the energy reservoir to support self-focusing in the filament core [14–16]. In the wake of the passing filament, aerosols in the vicinity of the filament are cleared for several milliseconds, resulting in a unique fog clearing hysteresis effect that can be quasi-sustained using high repetition rate pulse trains ($>$ 200Hz) to improve the transmission of subsequent pulses or secondary light sources [17–20]. Fog clearing has also been achieved using coherently-controlled molecular quantum wakes using a stacked fs-pulse train tuned to the molecular rotation of N_2, without having to generate a plasma through filamentation [21, 22].

In regards to the physical mechanism driving fog clearing, several studies have shown that micrometer-sized droplets behave similarly to a focusing lens, where laser light is internally focused due to refraction occurring at the irradiated surface [23–25]. In the higher intensity filament core, internal ablation can occur within the droplet volume to form a rapidly expanding micro-cavity that bursts the droplet through optical shattering, feasibly improving transmission of subsequent pulses by reducing light scattering from larger particle surfaces [26, 27]. This concept has recently been extended to the region of the energy reservoir, where 5 µm droplets in the energy reservoir are also shown to undergo a weaker shattering effect at the rear surface of the droplet, managing to cause backwards displacement by several hundred micrometers relative to the beam axis [28].

Unlike particle interactions that occur from exposure

* klatty@ufl.edu

to the laser pulse, transverse displacement of particles away from the filament results from the pressure of the expanding plasma shockwave [29–31]. Recently, optically trapped silica microspheres were shown to experience forces on the order of nN at distances upwards of 5 mm away from the filament due to shockwave interactions [32]. The shockwave expands by several millimeters, and thus serves as the only applicable displacement mechanism of particles beyond the boundaries of energy reservoir, with a diameter typically on the order of a millimeter. Unlike the axial displacement of droplets through optical shattering, transverse particle displacement induced by the shockwave directly propels particles away from the beam path. Intuitively, while the shockwave may appear to impact fog clearing more significantly, the relative contribution to fog clearing from laser-particle and shockwave-particle clearing mechanisms is difficult to quantify in isolation as both phenomena occur simultaneously. Furthermore, given optical shattering greatly depends on the optomechanical properties of the particle interactive with the laser pulse, the displacement magnitude and vector for particles other than water droplets remains unclear. Thus, the clearing behavior of filaments interacting with atmospheric aerosols containing solid particles (e.g., sand, snow, soot, pollen, nuclear fallout, etc.) is largely a topic of conjecture.

In this study, optical trapping is used to isolate solid particles with sizes ranging from 2-6 µm positioned near a passing fs-filament. Both graphite and silica microparticles are trapped and studied to represent the cases of absorptive and transparent particles in the atmosphere, respectively. Time-resolved shadowgraphy is used to measure the particle displacement 200 µs after interacting with the filament, and the original position of the trapped particle is varied relative to the location of the filament core. The evolution of the filament shockwave is also capture using shadowgraph images to determine the position of the shockwave, where the shockwave is observed exceeding the boundaries of the energy reservoir within the first 1 µs. The shockwave is confirmed to induce transverse particle displacement away from the filament, even for particles located outside the boundaries of the energy reservoir. We found that filaments can clear solid particles through several mechanisms, including shockwave pressure, radiation pressure, particle de-agglomeration, and mass ejection caused by the mechanical damage to the particle morphology through optical damage and ablation.

II. EXPERIMENTAL METHODS

A. Time-resolved shadowgraphy

A simplified schematic of the experimental setup is shown in Fig. 1(a). A chirped pulse amplified Ti:Sapphire laser (Coherent Astrella) is used to generate 60 fs pulses at a center wavelength of 800 nm. The pulse energy is

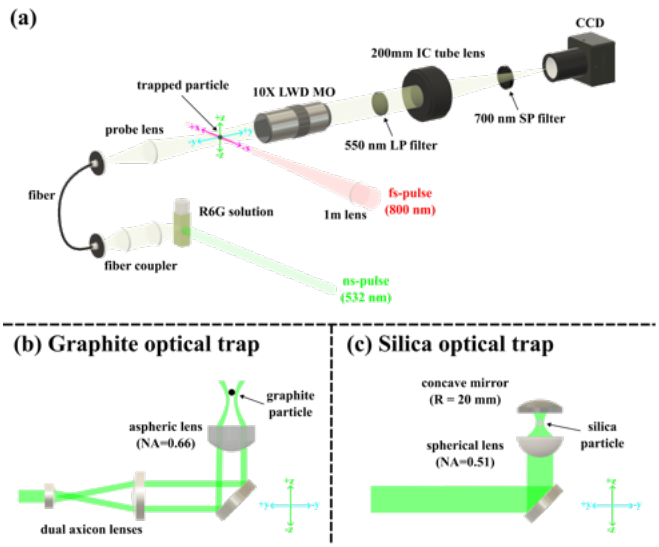

FIG. 1. (a) Simplified experimental setup used to measure particle displacement using time-resolved shadowgraphy. (b) A vertical hollow beam is generated using dual-axicon lenses to trap graphite particles. (c) A vertical confocal Gaussian beam generated using a concave mirror is used to trap silica particles.

adjusted to 3.6 mJ, yielding a peak power of 32 GW, exceeding the critical power for self-focusing in air (P_{cr}) by a factor of 6 [1]. Using a burn paper, only a single burn mark is found at the center using a 1-m focusing lens, indicating only a single filament is being formed with each laser pulse [33]. The repetition rate of the pulse train is set to 10 Hz to cleanly pass a single pulse through an optical shutter with an opening time of 6 ms (Uniblitz VS25, Vincent Associates).

Time-resolved shadowgraphy of trapped particles is performed using the fluorescence from a dilute rhodamine 6G (R6G) ethanol solution as probe source, pumped using a Q-switched Nd:YAG laser (Surelite-II, Amplitude) with the fundamental wavelength frequency doubled to 532 nm. The short-lived fluorescence of R6G produce shadowgraph images free of coherence artifact noise with time resolutions comparable to the pulse duration of the pump laser. Given the pulse duration of the Nd:YAG laser is 7 ns and the molecular fluorescence lifetime of R6G is 3.7 ns, the total fluorescence duration to yield time-resolved images is estimated to be ∼11 ns [34]. The R6G fluorescence from a cuvette is coupled into a single-mode fiber and a plano-convex lens (probe lens) is used to form an image of the fiber output near the trapping region. The particle shadows are imaged on an externally triggered CCD camera (Mightex) using a 10× long working distance infinity-corrected microscope objective and a conjugate $f = 200$ mm infinity-corrected tube lens. Laser light at 532 nm and 800 nm is blocked using a 550 nm long-pass filter and a 750 nm short-pass filter, respectively. The ns-laser is externally triggered from the fs-laser output pockel cell with an interpulse delay of

200 µs.

Shadowgraph images of the filament shockwave are captured by mounting a machine vision lens (MVL50M23, Navitar) to the CCD, yielding a magnification of $M = 0.903$. The position of the probe lens is adjusted to illuminate a larger area to accomodate the larger field-of-view. Each image is presented as a 100-shot average and are post-processed through background subtraction, normalization, and a Gaussian blur filter to help extract the edges of the shockwave.

B. Optical trapping

For trapping, a CW 532-nm laser (Cobolt Samba, Hübner Photonics) is used with a maximum power of 1 W. Particles are trapped in a custom 3D-printed chamber with small openings to pass the filament through without clipping or damaging the chamber. Particles are inserted using a pipette, with new particles being inserted periodically throughout the measurements. The chamber is decontaminated in an ultrasonic cleaner when changing out particles. The particle position is monitored in real-time using a de-magnified CCD camera (not shown in Fig. 1(a)) and shadowgraph images.

Graphite particles (3-5 µm) are photophoretically trapped using a vertical hollow beam formed with dual-axicon lenses, focused using an aspheric lens with a numerical aperture (NA) of 0.66 as shown in Fig. 1(b). The aspheric lens is mounted on a vertical translation stage, such that the height of the particles can be adjusted. Photopheretic trapping using a dual-axicon hollow beam has a tendency to trap multiple particles along the walls of the beam profile, in which case the most stable particle is isolated by slowly reducing the beam power [35].

Silica particles (2-6 µm) are trapped using a confocal trapping configuration shown in Fig. 1(c), where a Gaussian beam is focused upwards using a plano-convex lens with a NA of 0.51 that is refocused downwards using a concave spherical mirror ($f = 10$ mm). By refocusing the beam downwards, the upwards radiation pressure is counteracted to yield a dominant gradient force that stabilizes particles near the confocal region. The height of the confocal trapping region is adjusted by jointly moving both the lens and mirror. However, the particle position is not manipulated once they have been trapped as slight movements easily destabilize the particle, and thus particles cannot be precisely positioned.

III. RESULTS AND DISCUSSION

A. Graphite displacement

Graphite particles displaced by the filament are shown in Fig. 2, where displacement is measured 200 µs after the passage of the filament. Graphite particles are trapped using the hollow beam configuration depicted in Fig. 1(b), and the position is manipulated with a vertical micrometer stage relative to the beam path of the filament. Starting from the most intense region of the filament core, the particles are positioned above and away from the filament at 100 µm increments until the particles are no longer expelled from the trap at 500 µm. The depth of field is approximately 3.6 µm, and thus many of the particles appear out of focus after they are displaced by the filament.

Particles trapped near the region of the filament core (0-100 µm) in Fig. 2(a,b) are removed from the field-of-view (626×501 µm) without traces of fragments. Similar observations are reported for water droplets, where droplets placed 100 µm from the filament are completely removed from displacement images through optical shattering and vaporization [28]. The intensity of the fs-pulse is the highest within the intensity-clamped filament core, and thus particles located within this region as in Fig. 2(a) are susceptible to morphological changes through laser ablation or damage. For graphite, damage to surface morphology can occur at laser energy fluences as low as 100 mJ/cm ^{2} using fs-pulses, with several studies reporting mass removal through the ejection of nanoclusters induced by strong laser-induced vibrations in the lattice structure [36–38]. At higher energy fluences exceeding 1 J/cm^2, mass removal through ablation can occur and result in particle dissociation [36].

In order to compare the laser energy fluence of the filament to the damage and ablation threshold of graphite, a burn paper is used in the trapping region to measure the dimensions of the filament core and the surrounding energy reservoir, as shown in Fig. 3(a). The diameter of the filament core and the energy reservoir is measured to be 120 µm and 640 µm, respectively. It is noted that the full-width at half-maximum diameter (FWHM) of the filament core would be lower than the measured diameter apparent on the burn paper. For the purpose of discussion, 120 µm will be assumed for the filament core diameter as a conservative estimate for the laser energy fluence. The 1-m external focusing lens used in this experiment contributes to the beam convergence and results in a clamped intensity of 1.4×10^{14} W/cm^2, such that the average energy fluence of the filament core is approximately 9.5 J/cm^2 for a Gaussian beam [39]. This far exceeds the ablation threshold of graphite, and thus particles in the core are expected to dissociate through direct laser exposure and result in significant displacement through mass ejection of fragments. Under similar filament energy fluence conditions, emissions from the C_2 Swan system and CN violet system have been observed from ablating solid graphite samples as a result of vapor phase mixing of C_2 with atmospheric species, supporting graphite particles in the filament core can experience mass removal through ablation [40].

Particles residing between 200-300 µm away from the filament core as in Fig. 2(c,d) are firmly in the region of the energy reservoir and experience both axial displacement along the beam path and transverse displacement

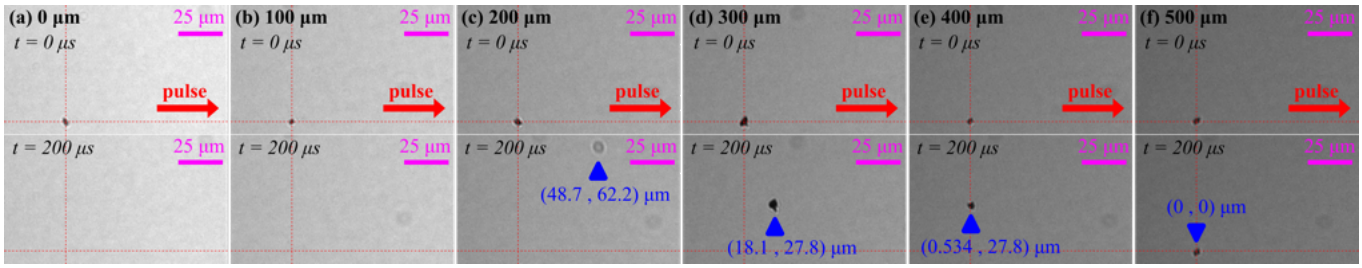

FIG. 2. Graphite particles displaced 200 μs after interacting with a passing filament, placed (a) 0 μm, (b) 100 μm, (c) 200 μm, (d) 300 μm, , (e) 400 μm, and (f) 500 μm away from the filament core.

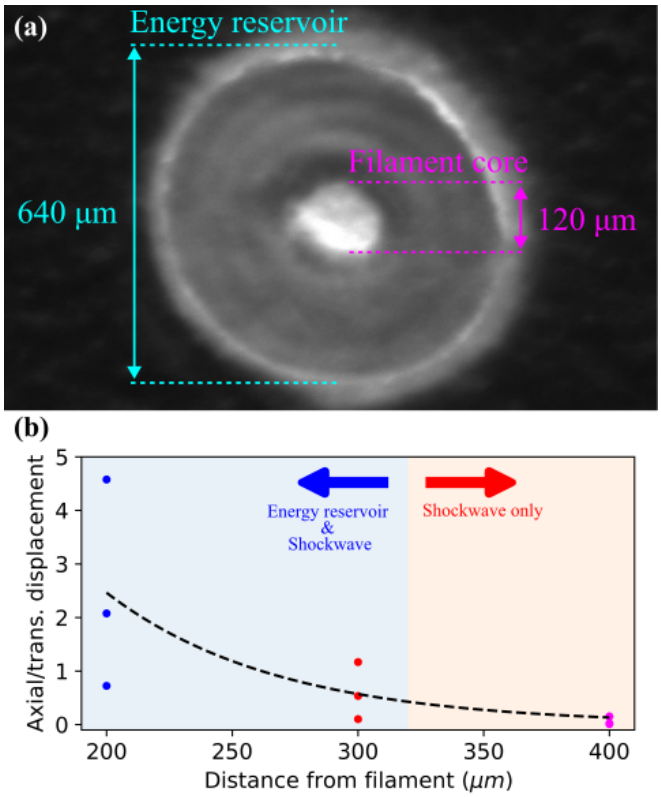

FIG. 3. (a) Transverse profile of the filament core and energy reservoir measured using a burn paper. (b) Axial-to-transverse displacement ratio measured for three different graphite particles trapped 200, 300, and 400 μm away from the filament core. Particles beyond the boundaries of the energy reservoir (>320 μm) only experience transverse displacement from the shockwave, resulting in a displacement ratio close to zero. An exponential function is fitted to guide the eye.

away from the filament. The axial displacement is caused by interactions at the particle surface exposed to the light of the reservoir, such that particles located outside the radius of the energy reservoir (320 μm) do not experience any axial displacement, as in cases of Fig. 2(e,f). Given the energy fluence and dimensions of the filament core, approximately 50% of the pulse energy (1.8 mJ) constitutes the energy reservoir, neglecting significant losses from air ionization. For an energy reservoir diameter of 640 μm with an inner hole representative of the filament core, the average energy fluence is ≈0.84 J/cm^2 and the energy fluence is expected to decrease closer to the outer boundaries of the energy reservoir [41, 42]. As such, particles closer to the filament core experience a higher energy fluence and are displaced further along the beam path. To demonstrate, three different graphite particles are placed 200, 300, and 400 μm from the filament core (9 total particles), and the ratio between the axial and transverse displacement is measured in Fig. 3(b). Axial displacement through laser-induced forces predominate closer to the filament core due to the higher energy fluences. Conversely, particles outside of the boundaries of the energy reservoir experience negligible axial displacement such that only transverse shockwave-induced forces remain to displace the particles away from the filament.

The force induced by radiation pressure is expected to be a dominant contributor to the axial displacement of particles. Approximating the graphite particles as a completely absorptive and spherical body, the radiation pressure is $F_{rp} = IA_p/c$, where I is the irradiance of the light source, A_p is the cross-sectional area of the particle, and c is the speed of light. Based on the shadowgraph images, most of the trapped graphite particles have diameters ranging from 3-5 μm, resulting in a radiation pressure force ranging from 2.8-7.8 mN given the average fluence of the energy reservoir. The force from radiation pressure calculated here is a million times stronger than the reported transverse force induced by the shockwave for 4.82 μm silica placed 1 mm away from the filament, measured to be on the order of several nN [32]. For further comparison, the optical trapping laser with a NA of 0.66 at maximum power imparts a radiation pressure force of only 0.32 μN which is sufficient to result in visible acceleration of particles during the trapping procedure.

The shockwave expands far beyond the boundaries of the energy reservoir, expanding to a radius of >1 mm within 2 μs as shown in Fig. 4. As such, particles located more than 320 μm away from the filament will only experience a transverse shockwave-induced force as in the case of Fig. 2(e). The three particles measured at 400 μm in Fig. 2(e) are displaced by 24-35 μm by the shockwave alone. Relative to the dimensions of the fila-

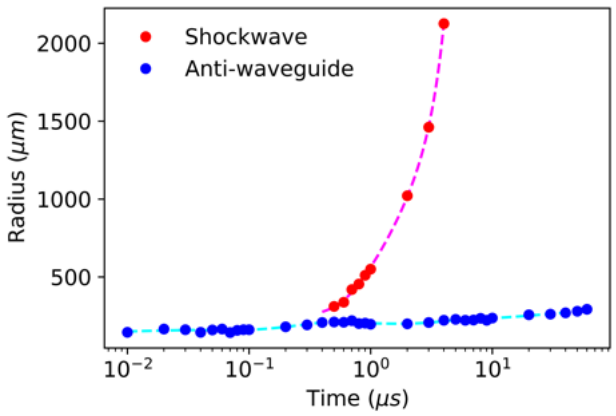

FIG. 4. Evolution of the filament shockwave and anti-waveguide thermal channel captured using time-resolved shadowgraph images. Spline models are fitted to each trend to guide the eye [47].

ment core (120 µm), the measured displacement of particles by the shockwave indicates filaments are capable of clearing air channels devoid of atmospheric debris to improve transmission of subsequent fs-pulses or secondary light sources. However, the shadowgraph images also reveals a persisting thermal anti-waveguides, which to the detriment of transmitting light through the cleared air channel, will refract light outwards without the use of structured waveguides [29, 43–46].

The images in Fig. 2(c,d) and the particle images used in Fig. 3(b) do not show indication of fragmentation in the particle morphology. It is possible that nanoclusters are ejected from the irradiated surface but are simply unresolved or out of focus, given the energy fluence of the energy reservoir exceeds the damage threshold for graphite reported to result in mass ejecta in solid samples [36–38]. However, the filament is found to be capable of breaking apart larger particle agglomerates as shown in Fig. 5(a,b). The individual fragments ejected from the agglomerates are displaced further from its original position the closer they are to the filament core, indicating de-agglomeration is driven mainly by direct exposure to laser light. This is further supported by the axial to transverse displacement ratios in Fig. 3(b), where a ratio larger than 1 indicates radiation pressure (axial displacement) imparts more energy to the particles than the shockwave (transverse displacement). Agglomerates outside of the energy reservoir as in the case of Fig. 5(c) are transversely displaced by the shockwave alone similar to the single particles in Fig.2(e), but remain largely intact. Acceleration from both radiation pressure and shockwave pressure are inversely proportional to the diameter of the particle, and thus de-agglomeration is expected to improve the particle displacement induced by subsequent pulses.

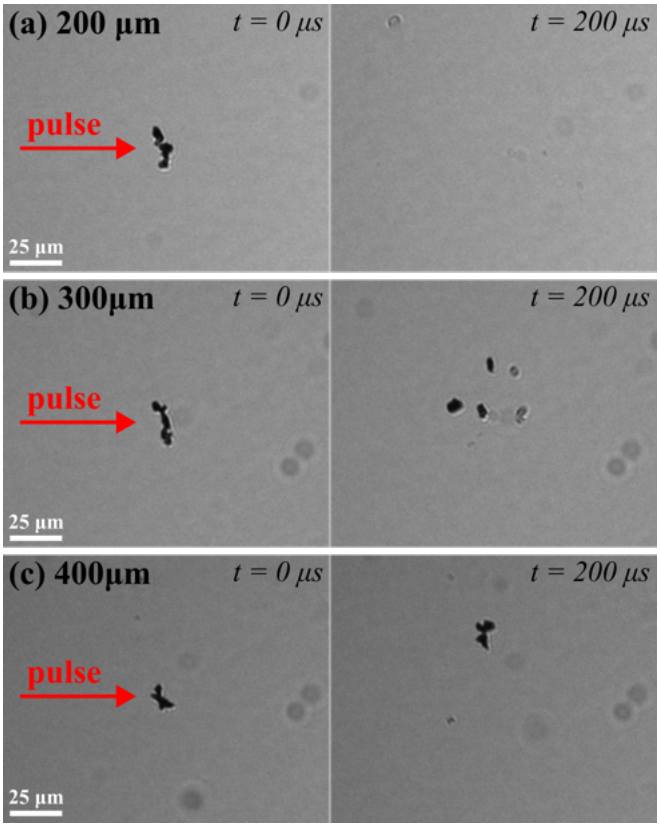

FIG. 5. Graphite de-agglomeration imaged 200 µs after interacting with a passing filament for particles positioned (a) 200 µm and (b) 300 µm from the filament core. At (c) 400 µm, the agglomerate is outside the boundaries of the energy reservoir and only experience transverse displacement from the shockwave.

B. Silica displacement

Silica microspheres (2-6 µm) are trapped using the confocal trapping configuration shown in Fig. 1(c) with a Gaussian beam. The position of the particle is no longer manipulated but instead, particles are trapped near the filament core and the relative distance to the filament is measured. The density of silica and graphite is 2.65 g/cm^3 and 2.26 g/cm^3, respectively. Given the similar particle size distributions, the mass of each individual particle is comparable. Characteristic displacement behaviors for silica are selected and presented in Fig. 6.

Similar to graphite, the silica particles experience outward transverse displacement from interacting with the shockwave. The silica particle 64 µm away from the filament core in Fig. 6(a) is removed from the field-of-view much like graphite in Fig. 2(a,b), possibly as a result of ablation. The abalation and damage threshold of silica is higher than graphite at 3.5 J/cm^2 and 2.5 J/cm^2, respectively [48]. Nonetheless, the average fluence of the filament core (9.5 mJ/cm^2) is still higher than the ablation threshold of silica, and thus particle dissociation is

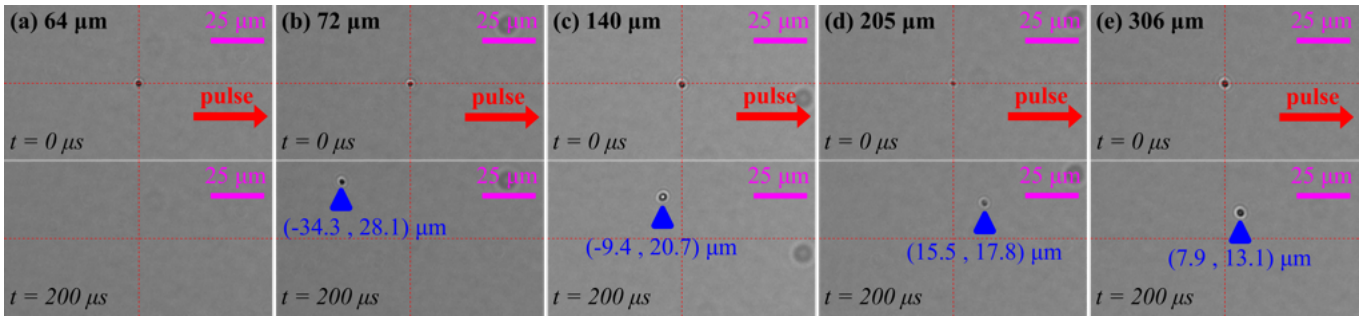

FIG. 6. Silica particles displaced 200 µs after interacting with a passing filament. The initial distance to the filament core is measured to be (a) 64 µm, (b) 72 µm, (c) 140 µm, (d) 205 µm, , (e) and 306 µm.

expected to occur.

Particles located 72-140 µm from the filament core are axially displaced backwards as shown in Fig. 6(b,c). This behavior is similar to optical shattering observed for water droplets caused by cavitation and ejection of mass from the rear surface of the droplet, resulting in backward axial displacement [28]. Both silica and water are mostly transparent to 800 nm laser light such that a similar optical shattering phenomenon is feasible to occur; however, a higher energy fluence is required to shatter silica as mass ejection cannot occur by disrupting surface tension, and would instead require morphological damage to occur close to the rear surface of the particle The average fluence of the energy reservoir (0.84 mJ/cm^2) is lower than the damage threshold of silica (2.5 mJ/cm^2), and thus the irradiated front surface of the particle is expected to remain intact. Light irradiating the front surface of the silica particle is expected to internally focus, increasing the energy fluence as the light propagates through the particle towards the rear surface. To estimate the fluence at the rear surface, silica microspheres are modeled using ray-transfer matrices for a thick lens with a radius of curvature equivalent to the particle radius with incident parallel rays. Assuming a constant transmission of 90%, the energy fluence at the rear surface is greater by a factor of 6.26 compared to the front irradiated surface, such that the energy reservoir fluence of 0.84 mJ/cm^2 incident at the front surface will be focused and increased to 5.3 mJ/cm^2. The fluence at the rear surface is higher than both the damage and ablation threshold of silica, supporting silica particles can eject mass localized near the rear surface to undergo optical shattering and propel the particle backwards.

Particles that are not optically shattering are axially displaced along the direction of the beam path as shown in Fig. 6(d,e). Without mass being ejected at the rear surface, backwards displacement cannot occur, leaving only the forward momentum imparted from scattered light. Silica particles in Fig. 6(d,e) are not displaced as far as graphite particles in Fig. 2(c,d) at similar distances from the filament core, indicating radiation pressure is lower for silica and other transparent particles. The reflected light at the particle surface results in radiation pressure that is twice as strong compared to absorbed light. Assuming negligible contribution from absorption and 10% reflectivity, the radiation pressure force experienced by silica particles is approximately a factor of 5 lower than graphite particles of equivalent size. Thus, particles that are transparent to the laser light and remain intact after exposure are expected to experience limited axial displacement compared to absorptive particles.

IV. CONCLUSION

Using time-resolved shadowgraph images of displaced optically trapped particles, laser filaments are demonstrated to be capable of clearing solid atmospheric debris consisting of micrometer-sized particles. Particles are displaced in both axial and transverse directions from laser-induced forces and the shockwave-induced force, respectively. The shockwave rapidly propagates beyond the boundaries of the energy reservoir and is capable of displacing particles by more than 10 µm, suggesting the filament can clear a channel larger than the diameter of the energy reservoir (640 µm) to improve transmission of subsequent pulses or secondary light sources. Axial displacement along the axis of the beam path is driven by interaction of particles with the high-intensity region of the filament core or the low-intensity region of the energy reservoir from direct laser exposure. As a result, the optical properties of the particle will heavily influence clearing mechanisms induced by laser interactions, which is demonstrated using graphite and silica particles to represent absorptive and transparent atmospheric debris. Absorptive particles will experience localized energy deposition at the irradiated surface to propel the particles along the beam path through mass ejection and radiation pressure. Furthermore, it is shown that the energy fluence of the energy reservoir is sufficiently high to break apart graphite particle agglomerates. Given acceleration from the shockwave and radiation pressure is inversely proportional to the particle size, de-agglomeration is expected to improve debris clearing by reducing the particle size distribution for subsequent pulses. Transparent par-

ticles can internally focus light to expel mass from the rear surface of the particle through ablation or mechanical damage, propelling the particle backwards against the beam path through optical shattering. Optical shattering is observed to occur only for particles close to the filament core where the energy fluence is expected to be higher than the ablation or damage threshold of the particle after internal focusing. Silica particles further away from the filament core (>200 µm) are propelled forward along the beam path like graphite, indicating the particle is largely unaffected by optical shattering leaving only the forward momentum imparted from scattered light. Given the shockwave directly pushes particles away from the filament, its implication with regards to atmospheric particle clearing is intuitive. Over several shots, transmission is expected to improve as long as the period of the pulse train is shorter than the recovery time of the aerosol. However, the consequence of axially displacing particles along the beam path through radiation pressure and optical shattering largely remains unknown for both droplets and solid particles. Given axial forces are increased at higher energy fluences, particle concentrations are expected to be reduced closer to the filament core as they are axially displaced to lower fluence regions; however, accurately determining particle transport over several shots would require complete knowledge of the energy distribution along the length of the filament. Furthermore, while two extreme cases are presented by investigating the axial displacement between graphite and silica, realistically most atmospheric particles are semi-transparent or semi-absorptive and would require further study to characterize their displacement mechanisms in a laser filament.

ACKNOWLEDGMENTS

This document is the result of research funded partially by the Department of Defense Science, Mathematics, and Research for Transformation (SMART) Scholarship-for-Service Program; US Department of Energy (DOE) National Nuclear Security Administration Consortium for Nuclear Forensics award number DE-NA0004142; and Defense Threat Reduction Agency award number HDTRA1-20-2-0002. The content of the information does not necessarily reflect the position or the policy of the federal government, and no official endorsement should be inferred.

[1] W. Liu and S. L. Chin, Direct measurement of the critical power of femtosecond Ti:sapphire laser pulse in air, Optics Express **13**, 5750 (2005).

[2] A. Becker, N. Aközbek, K. Vijayalakshmi, E. Oral, C. Bowden, and S. Chin, Intensity clamping and refocusing of intense femtosecond laser pulses in nitrogen molecular gas, Applied Physics B **73**, 287 (2001).

[3] H. Xu, A. Azarm, J. Bernhardt, Y. Kamali, and S. Chin, The mechanism of nitrogen fluorescence inside a femtosecond laser filament in air, Chemical Physics **360**, 171 (2009).

[4] M. Mlejnek, E. Wright, and J. Moloney, Dynamic spatial replenishment of femtosecond pulses propagating in air, Optics Letters **23**, 382 (1998).

[5] Z. Hao, J. Zhang, X. Lu, T. Xi, Z. Zhang, and Z. Wang, Energy interchange between large-scale free propagating filaments and its background reservoir, Journal of the Optical Society of America B **26**, 499 (2009).

[6] T. Fujii, N. Goto, M. Miki, T. Nayuki, and K. Nemoto, Lidar measurement of constituents of microparticles in air by laser-induced breakdown spectroscopy using femtosecond terawatt laser pulses, Optics Letters **31**, 3456 (2006).

[7] J.-F. Daigle, P. Mathieu, G. Roy, J.-R. Simard, and S. Chin, Multi-constituents detection in contaminated aerosol clouds using remote-filament-induced breakdown spectroscopy, Optics Communications **278**, 147 (2007).

[8] Z. Zhang, N. Zhang, Y. Wang, B. Xie, Y. Xiang, J. Guo, B. Shang, L. Guo, X. Zhao, M. Xie, L. Lin, and W. Liu, Detection of 1.4 µg/m ^{3} Na^+ in aerosol at a 30 m distance using 1 kHz femtosecond laser filamentation in air, Optics Express **31**, 6464 (2023).

[9] K. S. Latty, M. Burger, J. Borrero, I. Jovanovic, and K. C. Hartig, Emission characteristics of bulk aerosols excited by externally focused femtosecond filaments, Optics Express **31**, 24652 (2023).

[10] J. Kasparian, M. Rodriguez, G. Méjean, J. Yu, E. Salmon, H. Wille, R. Bourayou, S. Frey, Y.-B. André, A. Mysyrowicz, R. Sauerbrey, J.-P. Wolf, and L. Wöste, White-light filaments for atmospheric analysis, Science **301**, 61 (2003).

[11] G. Mejean, J. Kasparian, J. Yu, S. Frey, E. Salmon, and J.-P. Wolf, Remote detection and identification of biological aerosols using a femtosecond terawatt lidar system, Applied Physics B: Lasers and Optics **78**, 535 (2004).

[12] H. L. Xu and S. L. Chin, Femtosecond laser filamentation for atmospheric sensing, Sensors **11**, 32 (2010).

[13] O. A. Bukin, M. Y. Babii, S. S. Golik, A. A. Il'in, A. M. Kabanov, A. V. Kolesnikov, Y. N. Kulchin, V. V. Lisitsa, G. G. Matvienko, V. K. Oshlakov, and K. A. Shmirko, Lidar sensing of the atmosphere with gigawatt laser pulses of femtosecond duration, Quantum Electronics **44**, 563 (2014).

[14] F. Courvoisier, V. Boutou, J. Kasparian, E. Salmon, G. Méjean, J. Yu, and J.-P. Wolf, Ultraintense light filaments transmitted through clouds, Applied Physics Letters **83**, 213 (2003).

[15] M. Kolesik and J. V. Moloney, Self-healing femtosecond light filaments, Optics Letters **29**, 590 (2004).

[16] A. Dubietis, E. Kučinskas, G. Tamošauskas, E. Gaižauskas, M. A. Porras, and P. Di Trapani, Self-reconstruction of light filaments, Optics Letters **29**, 2893 (2004).

[17] L. de la Cruz, E. Schubert, D. Mongin, S. Klingebiel, M. Schultze, T. Metzger, K. Michel, J. Kasparian, and J.-P. Wolf, High repetition rate ultrashort laser cuts a path through fog, Applied Physics Letters **109**, 251105 (2016).

[18] G. Schimmel, T. Produit, D. Mongin, J. Kasparian, and J.-P. Wolf, Free space laser telecommunication through fog, Optica **5**, 1338 (2018).

[19] A. Higginson, Y. Wang, H. Chi, A. Goffin, I. Larkin, H. M. Milchberg, and J. J. Rocca, Wake dynamics of air filaments generated by high-energy picosecond laser pulses at 1 kHz repetition rate, Optics Letters **46**, 5449 (2021).

[20] A. D. Koulouklidis, C. Lanara, C. Daskalaki, V. Y. Fedorov, and S. Tzortzakis, Impact of gas dynamics on laser filamentation THz sources at high repetition rates, Optics Letters **45**, 6835 (2020).

[21] M. C. Schroeder, I. Larkin, T. Produit, E. W. Rosenthal, H. Milchberg, and J.-P. Wolf, Molecular quantum wakes for clearing fog, Optics Express **28**, 11463 (2020).

[22] S. Zahedpour, J. Wahlstrand, and H. Milchberg, Quantum control of molecular gas hydrodynamics, Physical Review Letters **112**, 143601 (2014).

[23] W.-F. Hsieh, J.-B. Zheng, C. F. Wood, B. T. Chu, and R. K. Chang, Propagation velocity of laser-induced plasma inside and outside a transparent droplet, Optics Letters **12**, 576 (1987).

[24] J. C. Carls and J. R. Brock, Propagation of laser breakdown and detonation waves in transparent droplets, Optics Letters **13**, 273 (1988).

[25] J.-b. Zheng, W.-F. Hsieh, S.-c. Chen, and R. K. Chang, Temporally and spatially resolved spectroscopy of laser-induced plasma from a droplet, Optics Letters **13**, 559 (1988).

[26] A. Lindinger, J. Hagen, L. D. Socaciu, T. M. Bernhardt, L. Wöste, D. Duft, and T. Leisner, Time-resolved explosion dynamics of H_2O droplets induced by femtosecond laser pulses, Applied Optics **43**, 5263 (2004).

[27] C. Jeon, D. Harper, K. Lim, M. Durand, M. Chini, M. Baudelet, and M. Richardson, Interaction of a single laser filament with a single water droplet, Journal of Optics **17**, 055502 (2015).

[28] A. Goffin, J. Griff-McMahon, I. Larkin, and H. Milchberg, Atmospheric aerosol clearing by femtosecond filaments, Physical Review Applied **18**, 014017 (2022).

[29] N. Jhajj, E. Rosenthal, R. Birnbaum, J. Wahlstrand, and H. Milchberg, Demonstration of long-lived high-power optical waveguides in air, Physical Review X **4**, 011027 (2014).

[30] O. Lahav, L. Levi, I. Orr, R. A. Nemirovsky, J. Nemirovsky, I. Kaminer, M. Segev, and O. Cohen, Long-lived waveguides and sound-wave generation by laser filamentation, Physical Review A **90**, 021801 (2014).

[31] G. Point, E. Thouin, A. Mysyrowicz, and A. Houard, Energy deposition from focused terawatt laser pulses in air undergoing multifilamentation, Optics Express **24**, 6271 (2016).

[32] M. C. Schroeder, U. Andral, and J.-P. Wolf, Optomechanical expulsion of individual micro-particles by laser-induced shockwave in air, AIP Advances **12**, 095119 (2022).

[33] S. L. Chin, A. Brodeur, S. Petit, O. G. Kosareva, and V. P. Kandidov, Filament and supercontinuum generation during the propagation of powerful ultrashort laser pulses in optical media (white light laser), Journal of Nonlinear Optical Physics & Materials **08**, 121 (1999).

[34] K. A. Selanger, J. Falnes, and T. Sikkeland, Fluorescence lifetime studies of Rhodamine 6G in methanol, The Journal of Physical Chemistry **81**, 1960 (1977).

[35] T. Liu, X. Cheng, Q. Zhang, T. Zhang, and J. Bai, Improvement of the reproducibility in LIBS single levitated aerosol particle analysis based on particle size-selectivity of photophoretic optical trap, Talanta **268**, 125326 (2024).

[36] S. Amoruso, G. Ausanio, M. Vitiello, and X. Wang, Infrared femtosecond laser ablation of graphite in high vacuum probed by optical emission spectroscopy, Applied Physics A **81**, 981 (2005).

[37] M. Lenner, A. Kaplan, C. Huchon, and R. E. Palmer, Ultrafast laser ablation of graphite, Physical Review B **79**, 184105 (2009).

[38] A. A. Ionin, S. I. Kudryashov, S. V. Makarov, N. N. Mel'nik, P. N. Saltuganov, L. V. Seleznev, and D. V. Sinitsyn, Ultrafast femtosecond laser ablation of graphite, Laser Physics Letters **12**, 075301 (2015).

[39] S. I. Mitryukovskiy, Y. Liu, A. Houard, and A. Mysyrowicz, Re-evaluation of the peak intensity inside a femtosecond laser filament in air, Journal of Physics B: Atomic, Molecular and Optical Physics **48**, 094003 (2015).

[40] E. J. Judge, G. Heck, E. B. Cerkez, and R. J. Levis, Discrimination of composite graphite samples using remote filament-induced breakdown spectroscopy, Analytical Chemistry **81**, 2658 (2009).

[41] A. Couairon and L. Bergé, Light filaments in air for ultraviolet and infrared wavelengths, Physical Review Letters **88**, 135003 (2002).

[42] X.-L. Liu, W. Cheng, M. Petrarca, and P. Polynkin, Measurements of fluence profiles in femtosecond laser filaments in air, Optics Letters **41**, 4751 (2016).

[43] M. Alshershby, Z. Hao, A. Camino, and J. Lin, Modeling a femtosecond filament array waveguide for guiding pulsed infrared laser radiation, Optics Communications **296**, 87 (2013).

[44] M. Châteauneuf, S. Payeur, J. Dubois, and J.-C. Kieffer, Microwave guiding in air by a cylindrical filament array waveguide, Applied Physics Letters **92**, 091104 (2008).

[45] P. J. Skrodzki, M. Burger, L. A. Finney, R. Nawara, J. Nees, and I. Jovanovic, Millisecond-long suppression of spectroscopic optical signals using laser filamentation, Optics Letters **46**, 3777 (2021).

[46] S. B. Ali Reza, M. Burger, P. Bassène, T. Nutting, I. Jovanovic, and M. N'Gom, Generation of multiple obstruction-free channels for free space optical communication, Optics Express **31**, 3168 (2023).

[47] See Supplemental Material at inserturl for the images used to capture the evolution of the filament shockwave and thermal anti-waveguide channel. Each frame of the filament evolution is averaged over 100 shots and background substracted for better clarity prior to edge extraction.

[48] B. Chimier, O. Utéza, N. Sanner, M. Sentis, T. Itina, P. Lassonde, F. Légaré, F. Vidal, and J. C. Kieffer, Damage and ablation thresholds of fused-silica in femtosecond regime, Physical Review B **84**, 094104 (2011).